X-713-65-372



# THE MEASUREMENT AND APPLICATION OF THE QUANTUM YIELD OF SOLAR CELLS USING A FILTER TECHNIQUE





SEPTEMBER 1965

GODDARD SPACE FLIGHT CENTER
GREENBELT, MARYLAND

# THE MEASUREMENT AND APPLICATION OF THE QUANTUM YIELD OF SOLAR CELLS USING A FILTER TECHNIQUE

by

William G. Gdula
Daniel J. Gallagher
Radiometry Group
Thermal Systems Branch
Spacecraft Technology Division

September 1965

This work was supported by ART Work Unit Number 123-33-01 (Solar Cell Calibration Techniques).

Goddard Space Flight Center
Greenbelt, Maryland

# THE MEASUREMENT AND APPLICATION OF THE QUANTUM YIELD OF SOLAR CELLS USING A FILTER TECHNIQUE

by

William G. Gdula*
Daniel J. Gallagher
Radiometry Group
Thermal Systems Branch
Spacecraft Technology Division

## ABSTRACT



The measurement of absolute quantum yields of solar cells by means of narrow-band interference filters is described. Optical properties of the filters and representative experimental data obtained the application of the quantum yield measurements in radiation damage experiments, unique solar cell fabrication techniques and diffusion length measurements are briefly presented.

author

*Taag Designs, Inc. employee at GSFC – Contract # NAS5-2382.

# THE MEASUREMENT AND APPLICATION OF THE QUANTUM YIELD OF SOLAR CELLS USING A FILTER TECHNIQUE

## I. INTRODUCTION

In order to gain additional insight into the energy conversion process by photovoltaic solar cells, techniques and instrumentations have been developed to measure the absolute quantum yield. This term effectively describes the ability of the device to convert incident photon energies of specified wave length to electron-hole pairs capable of delivering power to an external load.

The measurement of absolute quantum yields presents some technical difficulties, primarily because the ultimate accuracy is dependent upon absolute radiance standards and non-selective calibrated detectors. Absolute quantum yield measurements have a greater physical significance and practical application than the usual relative measurements, even with the inherent accuracy limitations imposed by the use of radiance standards and absolute detectors. This becomes readily apparent when it becomes necessary to evaluate the performance of the energy conversion device after undergoing thermal vacuum cycling, varying fabrication processes such as diffusion at high temperatures, applications of anti-reflection coatings, surface sandblasting and chemical etching.

## II. FILTER DESCRIPTION

Narrow-band interference filters, manufactured by Balzers,[1] are presently being used in making the absolute quantum yield measurements. The wavelength range of these filters is from 400 nm to 1100 nm. The interference filter consists of a thin layer of transparent dielectric material with a vacuum deposited silver coating on both faces, the semi-reflecting silver layers and dielectric region is then covered with glass plates for protection. Figure 1 shows a typical filter construction. The optical thickness of the dielectric material determines the wavelength transmitted. When this optical separation is an effective half-wave length or multiple intergers thereof, relatively high transmission of the wavelength is realized. That portion of the optical spectrum which is not transmitted is reflected, with of course, small absorption losses.

[1] Balzers Aktiengesellschaft fur Hochvakuumtechnik und Dunne Schichten; Balzers, Furstentum, Liechtenstein.

A characteristic spectral transmission of the Balzers filters is shown in Figure 2. When the optical separation is one-half wavelength of the peak transmission, the filter is classified as a first order filter, when the spacing is two half wavelengths the classification is second order, etc. The Balzers filters are second order filters which are characterized by lower transmission and narrower bandwidth properties. Ideally, it is desirable to have filters with maximum transmission and minimum bandwidth properties. However, narrow bandwidths can only be achieved by increasing the thickness of the semi-reflecting layers which in turn reduces the transmission. Transmission and bandwidth properties of the filters have been measured and are given in Table 1. The derivation of the transmitted intensity is given by Airy's Formula[2]

$$I = \frac{T^2}{(1 - R)^2} \frac{1}{1 + 4R(1 - R)^2 \sin^2 1/2\delta} \quad (1)$$

where I = Percent of transmitted radiation
T = Percent of incident radiation transmitted by single semi-transparent film
R = Percent of incident radiation reflected by single semi-transparent film
$\delta$ = Phase difference between successive interfering wavelengths and is given by

$$\delta = \frac{4\pi d}{\lambda} (n - 2 - \sin^2 \theta + 2y)^{1/2} \quad (2)$$

Table I

| Wavelength nm | Transmission % | Bandwidth nm |
|---|---|---|
| 400 | 27.5 | 20 |
| 440 | 34.2 | 14 |
| 501 | 34.8 | 19 |
| 561 | 32.8 | 12 |
| 601 | 32.6 | 12.5 |
| 642 | 14.1 | 11 |

[2]Detection and Measurement of Infrared Radiation, Smith, Jones and Chasmar, Oxford Press, 1957.

Table I (Continued)

| Wavelength nm | Transmission % | Bandwidth nm |
|---|---|---|
| 742 | 39.0 | 14 |
| 802 | 33.5 | 11 |
| 848 | 37.8 | 14 |
| 904 | 36.5 | 13 |
| 948 | 39.1 | 13 |
| 1000 | 21.2 | 15 |
| 1100 | 38.5 | 20 |
| 1200 | 42.0 | 50 |

where d = Thickness of dielectric layer
n = Refractive index of dielectric layer
$\theta$ = Incident angle of radiation
y = Phase change on reflection at semi-reflecting layer.

As seen from Equation 2, normal incident radiation is a requisite in order to maintain consistent bandwidth and peak wavelength properties of the interference filter. Collimated radiation is used in the experimental setup to eliminate the dependence of the transmitted radiation as a function of angle of incidence.

In addition to the dependence of the filter properties on the incident angle of the radiation, the interference filter inherently has pass bands other than the fundamental. These pass bands are the result of the optical spacing of the semi-transparent films being multiples of the fundamental. All second order effects are removed from the Balzers filters by selective use of Corning glass color filters in the region of 400 nm to 1100 nm.

Other factors which must be considered when using this type of filter are: background transmission; and, transmission in the 300 nm region due to the optical characteristics of the evaporated films used. A Beckman DK-Z spectrophotometer was used to measure the background transmission of each filter and in no instance did it exceed 0.1%. The transmission properties at the thin films were measured in the UV region; each filter exhibited negligible transmission.

## III. EXPERIMENTAL PROCEDURE

In order to simplify the measurement taking and achieve greater accuracy, the interference filters were mounted on a rotating wheel assembly. A calibrated

thermopile, mounted in the center of the assembly, measures the monochromatic energy incident on the sample area. Several light sources were used in preliminary analysis but it was found that the xenon high-pressure, compact arc lamp proved superior to Hg and tungsten sources. The ability to achieve uniform collimated radiation and the greater continuum in the spectral energy distribution were the prime considerations in using xenon as the source of radiation.

Outputs of the thermopile at the discrete wavelengths are measured with a Keithley 149 millimicrovolt meter and displayed on a Hp 561 digital recorder. This instrumentation is mounted in a panel rack along with the filter wheel assembly, program control unit and an automatic I-V generator which are shown in Figure 3.

Rather than deal with relative energy levels in the measurement of the quantum yield a thermopile, which measures total energy, is used as the radiation detector. This enables the solar cells to be calibrated in absolute units of energy, that is, electron-hole pairs per incident photon. Absolute calibration of non-selective thermal radiation detectors is difficult and the calibration accuracy of the Eppley thermopile is no better than ±2%. This error is primarily a result of gold black reflectance and transmission properties. Also, the calibration constant assigned to the thermopile is an emf measured under radiation of an NBS carbon filament standard lamp with intensities from 42 to 87 $\mu$ watts/cm$^2$. The large dynamic range of radiation intensity levels, over five decades of variance place stringent requirements on detector linearity. The linearity measurement for the Eppley thermopile used, a twelve junction Bismuth Silver circular type, is shown in Figure 4, where the intensity is attenuated by use of neutral density screen-mesh filters.

When the quantum yield measurement, as a function of wavelength, is made, the thermopile calibration constant is the factor which determines the absolute level. Essentially, this constant determines the photon densities incident on the cell. The mean emf of the twelve junction thermopile used is 0.121 microvolts per microwatt per sq. cm. By converting the monochromatic thermal emf to corresponding eV energy, total photon flux, $N_o$, can be calculated. This is given by

$$N_{o(\lambda)} = \frac{CT\,6.24 \times 10^{12}}{\frac{hc}{\lambda}} \qquad (3)$$

where C = Thermopile calibration constant
T = Measured emf
$hC/\lambda$ = Photon energy

Once the photon flux is known the quantum yield can readily be calculated. The solar cell short-circuit current under monochromatic illumination, $i_\lambda$, which can be written as

$$i_\lambda = \int_0^D K(x)\, No\, (1 - R)\, e^{-\alpha x}\, dx \qquad (4)$$

where No = Monochromatic photon flux
$\alpha$ = Optical absorption coefficient
K(x) = Collection efficiency parameter
D = Solar cell thickness
R = Surface reflection coefficient

is measured and the ratio

$$QY = \frac{i_\lambda}{No_{(\lambda)}} \qquad (5)$$

is the ability of the P/N junction to collect the minority carriers created by the intrinsic absorption of the incident photon flux. The actual absorption and resultant collection process is dependent upon many variables including the optical absorption coefficient, minority carrier lifetime, effective mobility, temperature, impurity concentrations and impurity profile, junction depth, band gap, surface conditions and numerous fabrication process techniques.

A great deal of simplification and practical use of the quantum yield concept can be achieved by relying upon the experimental data and its proper interpretation.

## IV. EXPERIMENTAL RESULTS AND APPLICATION

The quantum yield of an N/P silicon solar cell is given in Figure 5. Here the absolute quantum yield has been corrected for surface reflection losses and the area covered by the electrode and grid structure, as can be seen in Figure 6, which shows the reflectance properties of a coated and a Si0 coated sample the current density can be increased by as high as 24% with the proper surface treatment. Overall power conversion of the RCA sample, which was used on the

Nimbus solar panel array, is 11.7%. The peak quantum yield is 94% which approaches the theoretical unity quantum yield concept. Current collection losses in the N region are primarily a result of surface recombination and low minority carrier lifetime due to the large impurity concentrations resulting from the junction formation process.

Electron-hole pairs which are generated within a diffusion length, L , of the junction can be collected and the quantum yield should be linear as a function of photon energies. This is clearly shown in Figure 7 where the quantum yield is linear from 550 nm to 900 nm. This figure also demonstrates the importance of absolute measurements when conducting a radiation damage experiment. It is seen that there is no "shift" in the spectral response; a prevalent notion engendered by the accepted use of normalized relative measurements, but a general degradation is shown in the longer wavelength regions. The same principle applies when speaking of blue-shifted and super-blue solar cells.

The decrease in the quantum yield at lower photon energies is given by the approximate relation:

$$QY = \frac{1}{1 + \frac{1}{\alpha(\lambda)L}} \qquad (6)$$

where $\alpha(\lambda)$ = optical absorption coefficient ($cm^{-1}$)

L = diffusion length (microns)

Once the quantum yield is plotted as a function of the optical absorption coefficient $\alpha$, the diffusion length of the minority carriers in the base region can be obtained from Equation 6 since at 50% quantum yield, $\alpha(\lambda) L = 1$. The optical absorption coefficient of silicon is plotted in Figure 8 and the quantum yield of drift field solar cells as a function of $\alpha$ is given in Figure 9. Diffusion lengths in samples with high quantum yields range from 120 to 210 microns. The cell shown in Figure 7 has an exceptionally long diffusion length, 210 microns, as a direct result of the high resistivity 200 ohm-cm base material.

Plotting the absolute quantum yield as a function of the optical absorption coefficient lends additional insight into electron-hole pair generation process in relation to the fabrication techniques used in making the solar cell. This is demonstrated in Figure 10 where the quantum yield is plotted as a function of diffusion time in the junction formation process.

## V. SUMMARY

As clearly evidenced by the multitude of its uses, the absolute quantum yield of solar cells measured by the narrow band interfence filters provides fundamental experimental data not only in the application but also in the direct control of the fabrication process involved in making the solar cell.

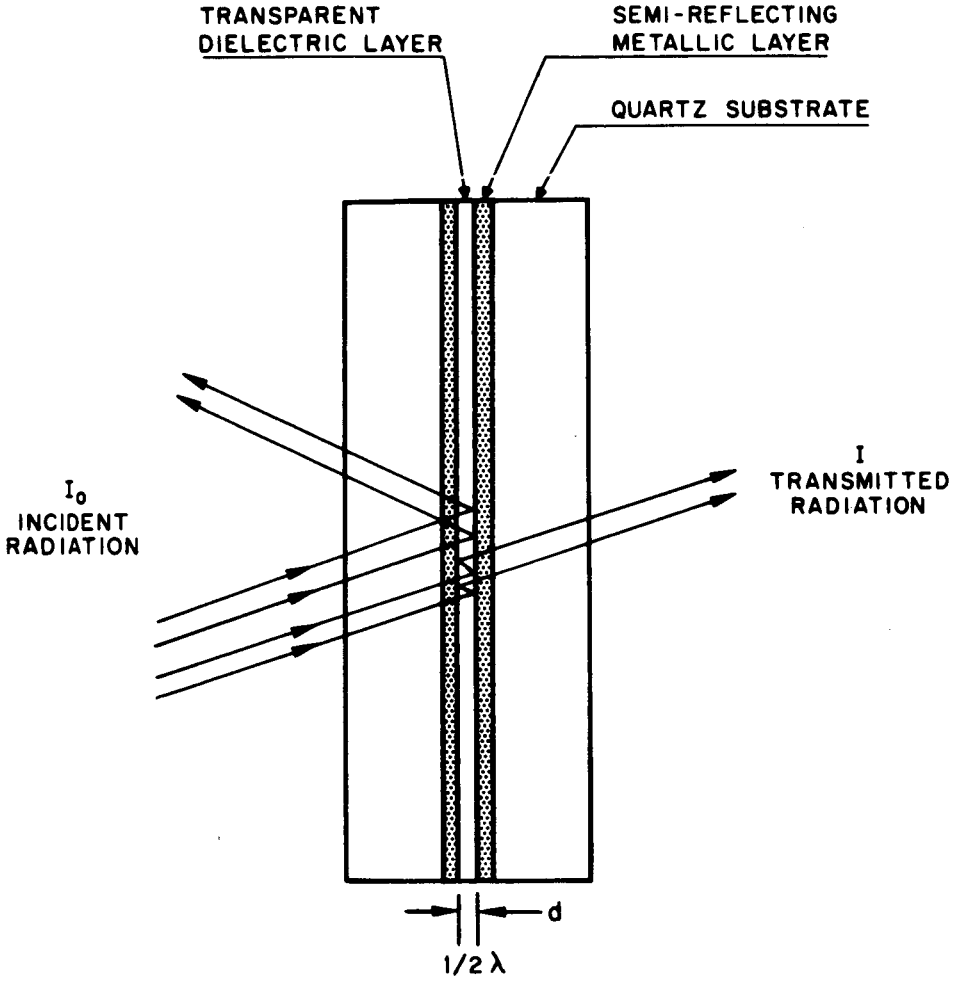


Figure 1–Interference Filter Cross-Section

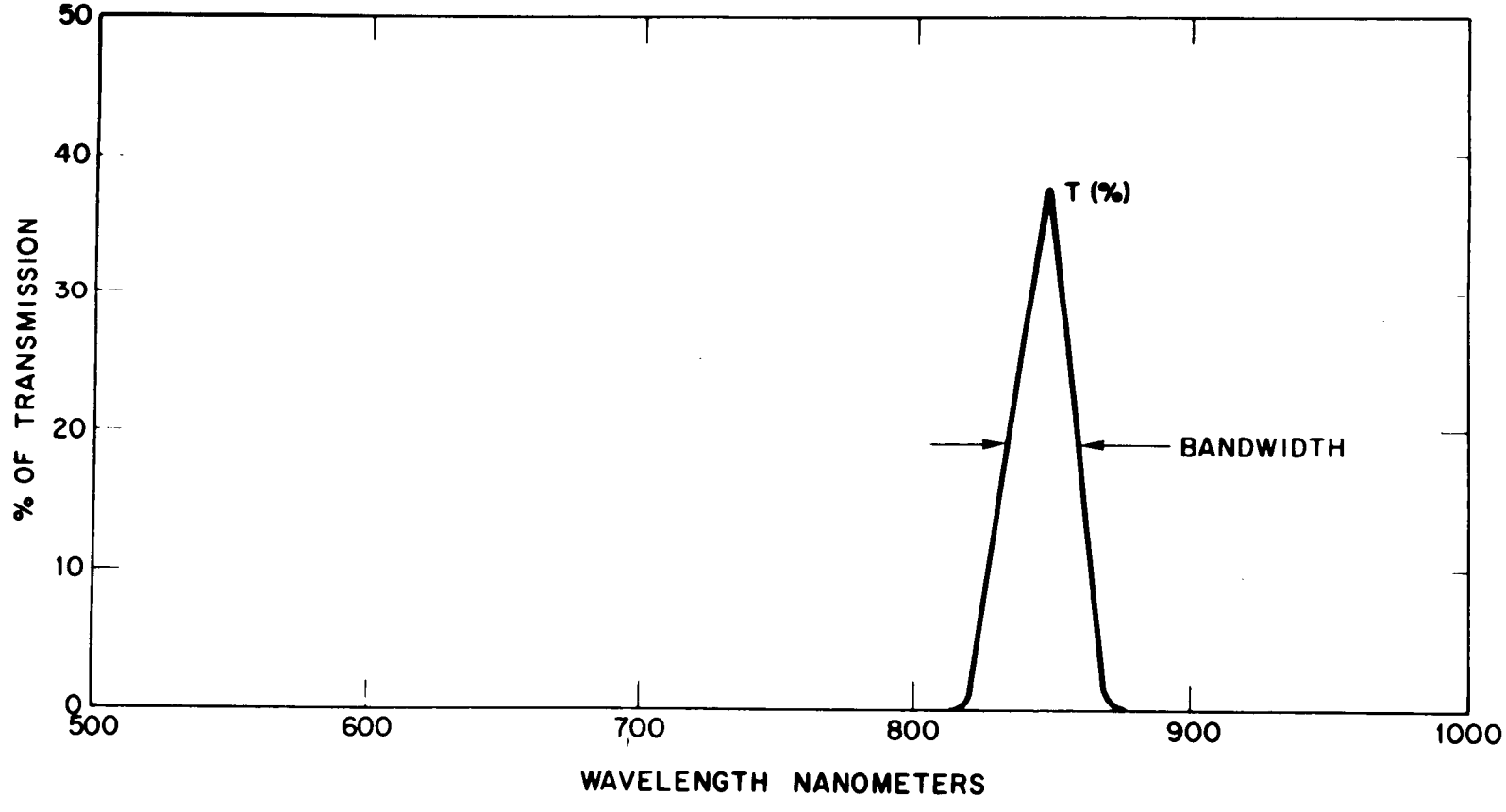


Figure 2–Spectral Transmission of Balzers Filter

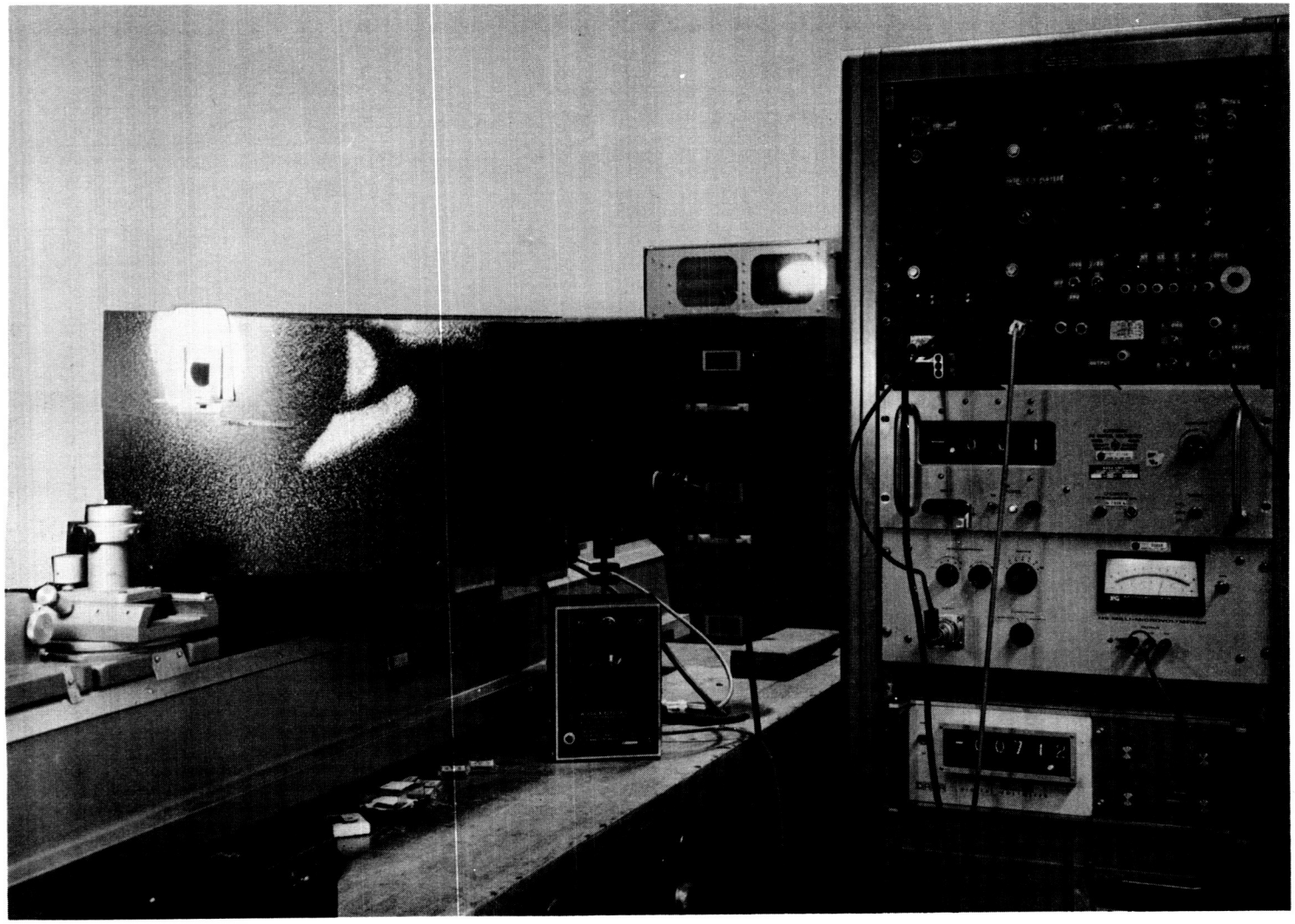

Figure 3–Filter Wheel Assembly and Instrumentation

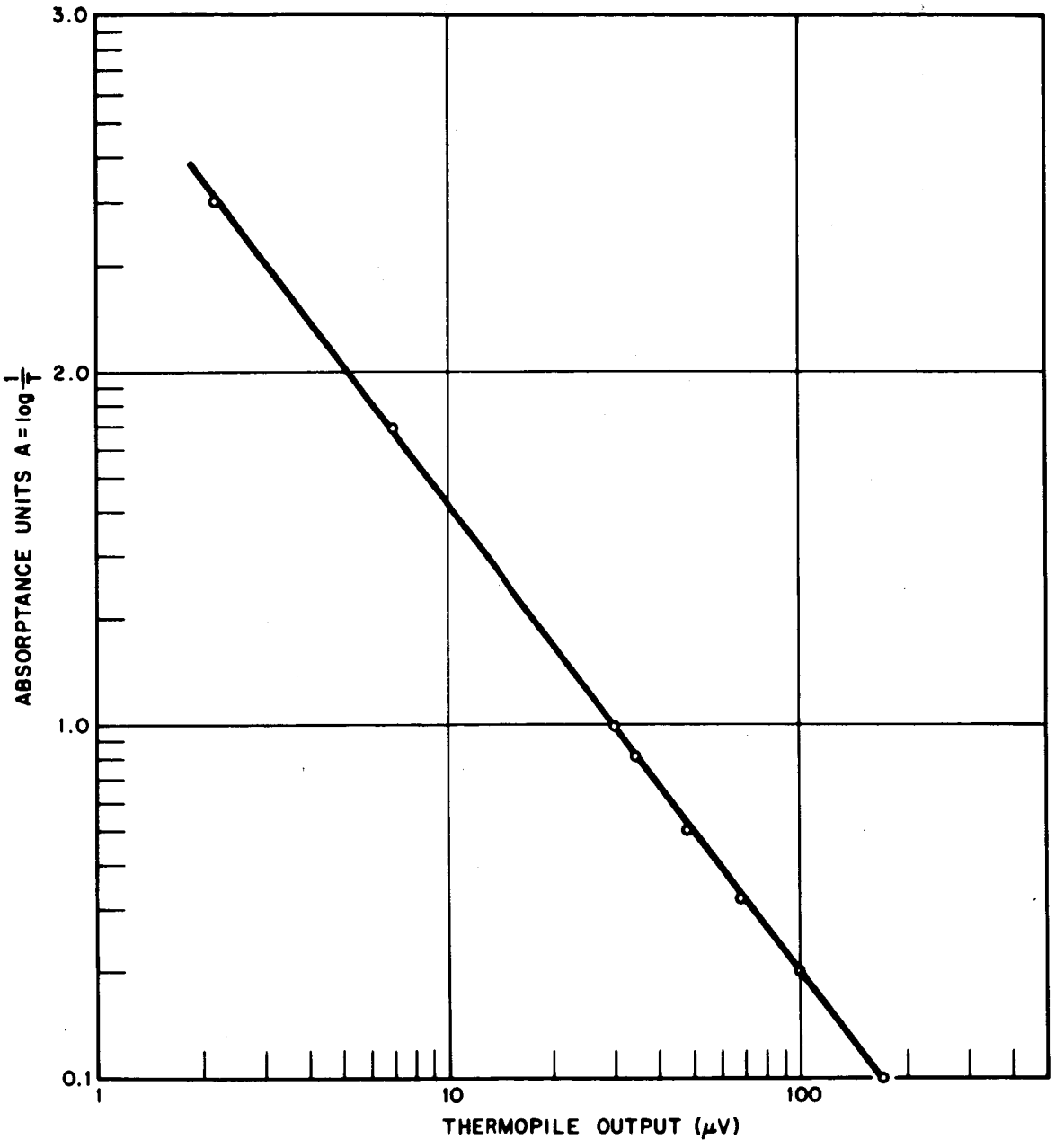


Figure 4–Thermopile Linearity

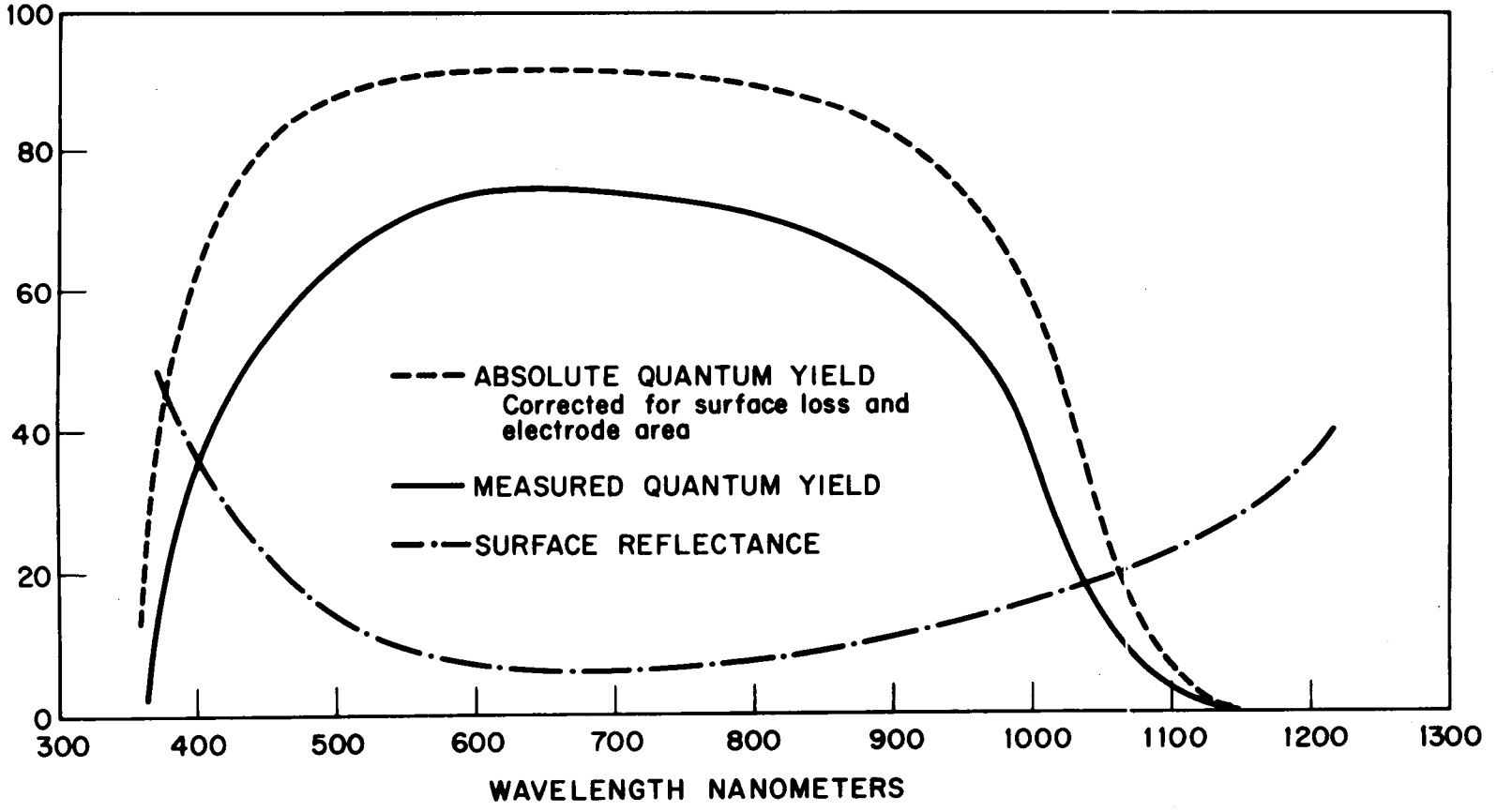


Figure 5–Quantum Yield, Silicon Solar Cell

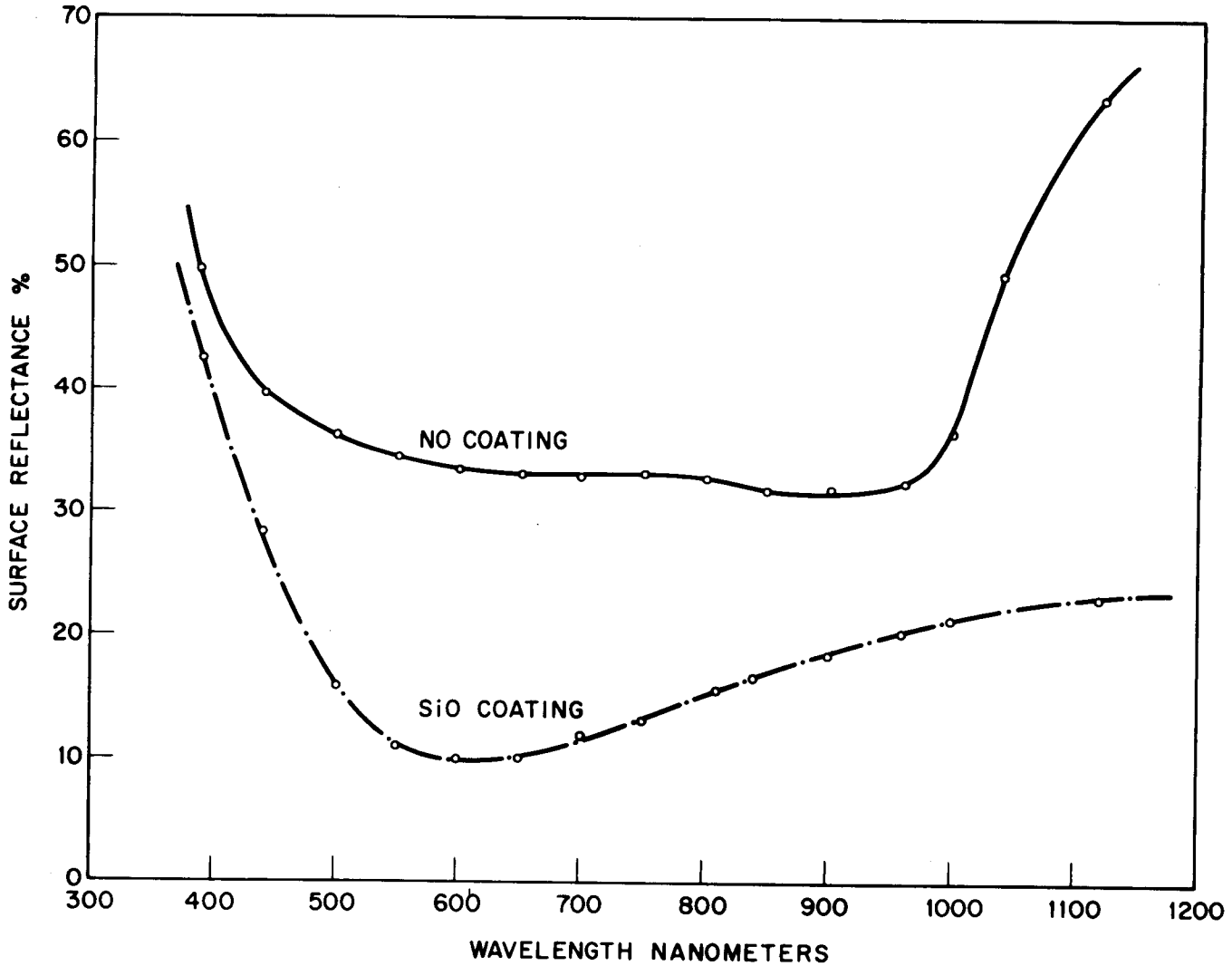


Figure 6–Surface Reflectance of Silicon Solar Cell

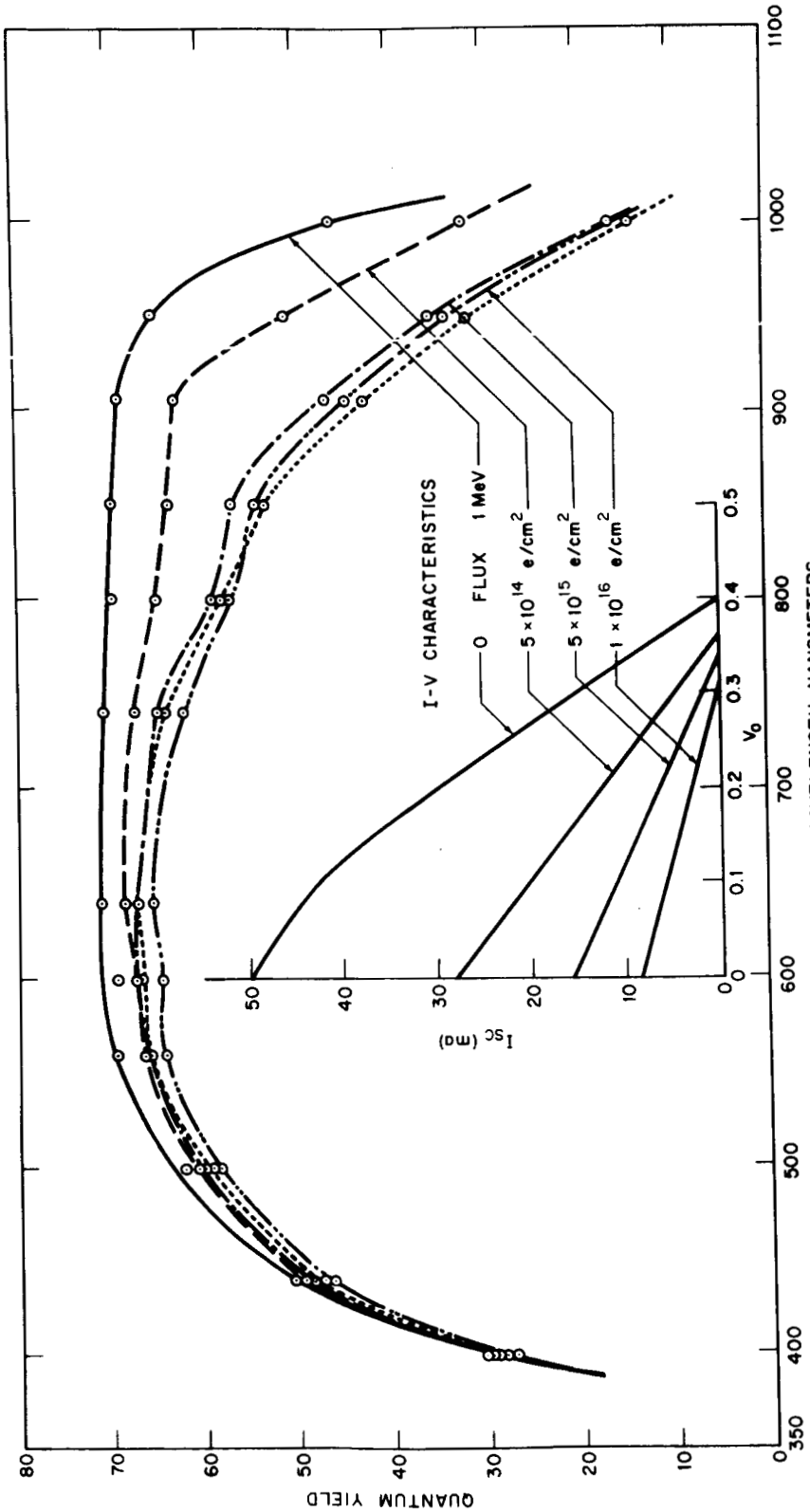


Figure 7–200 ohm-cm Silicon Solar Cell

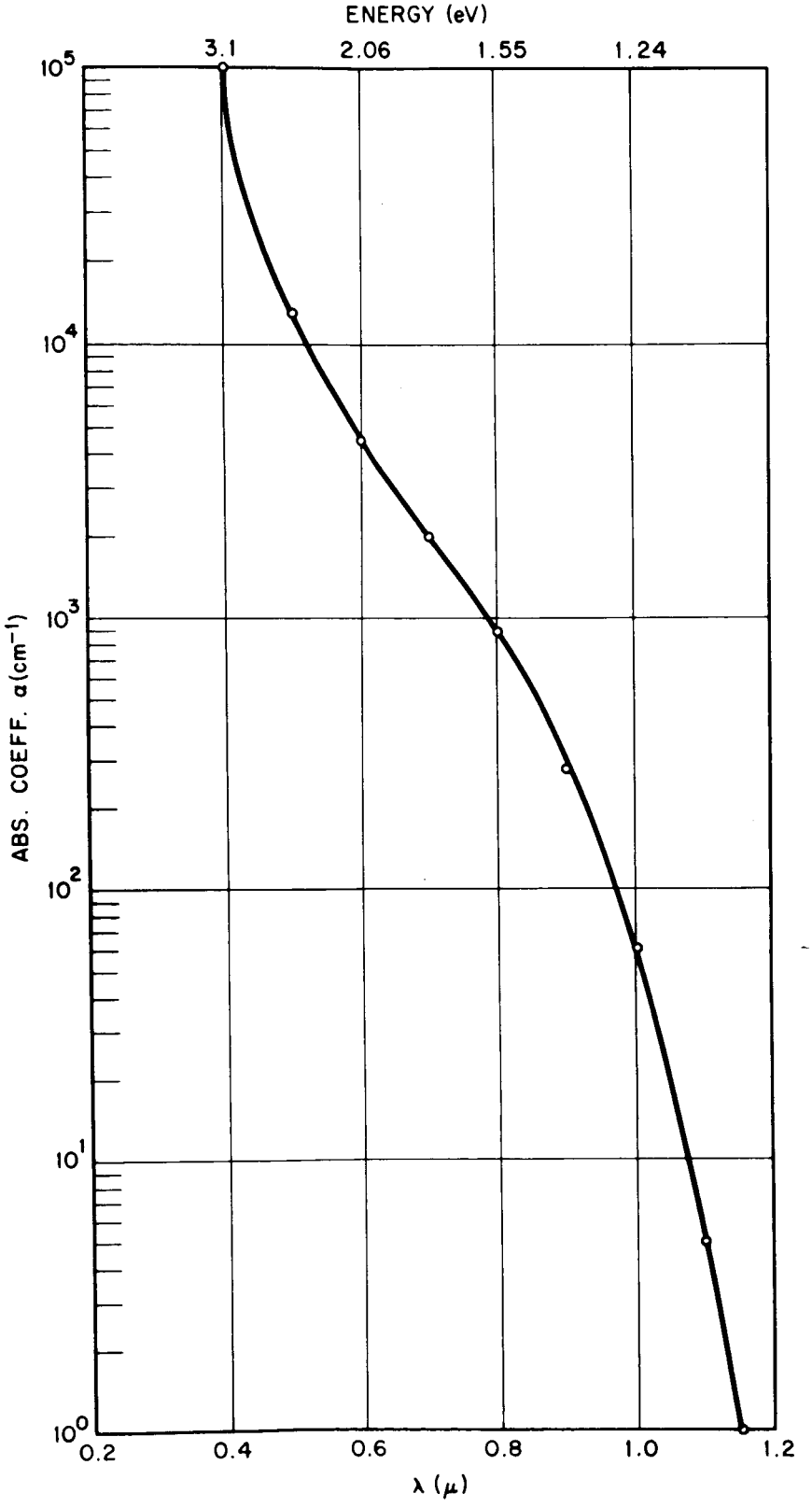


Figure 8–Optical Absorption Data (Fan, et al)

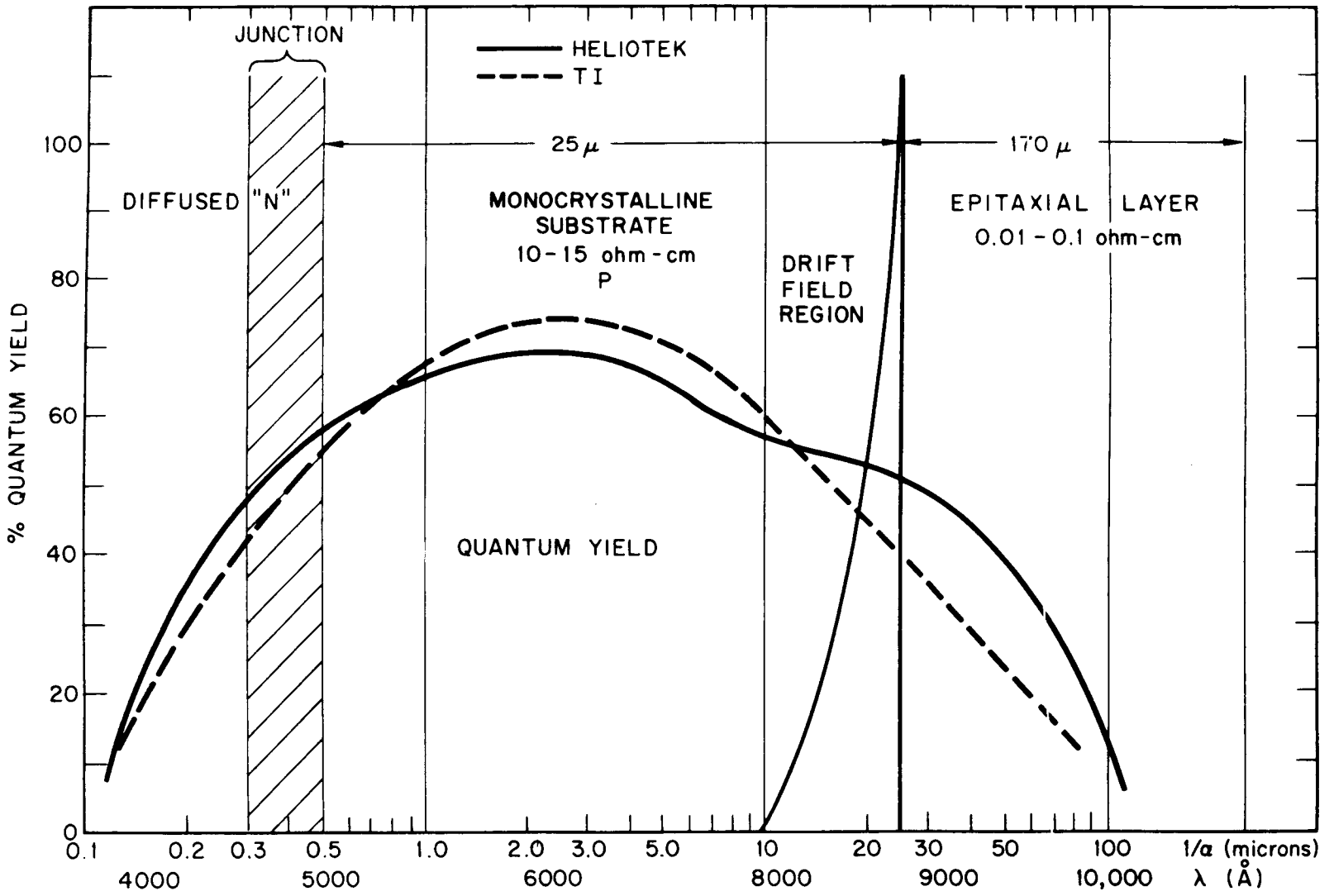


Figure 9–Quantum Yield as a Function of the Optical Absorption Coefficient

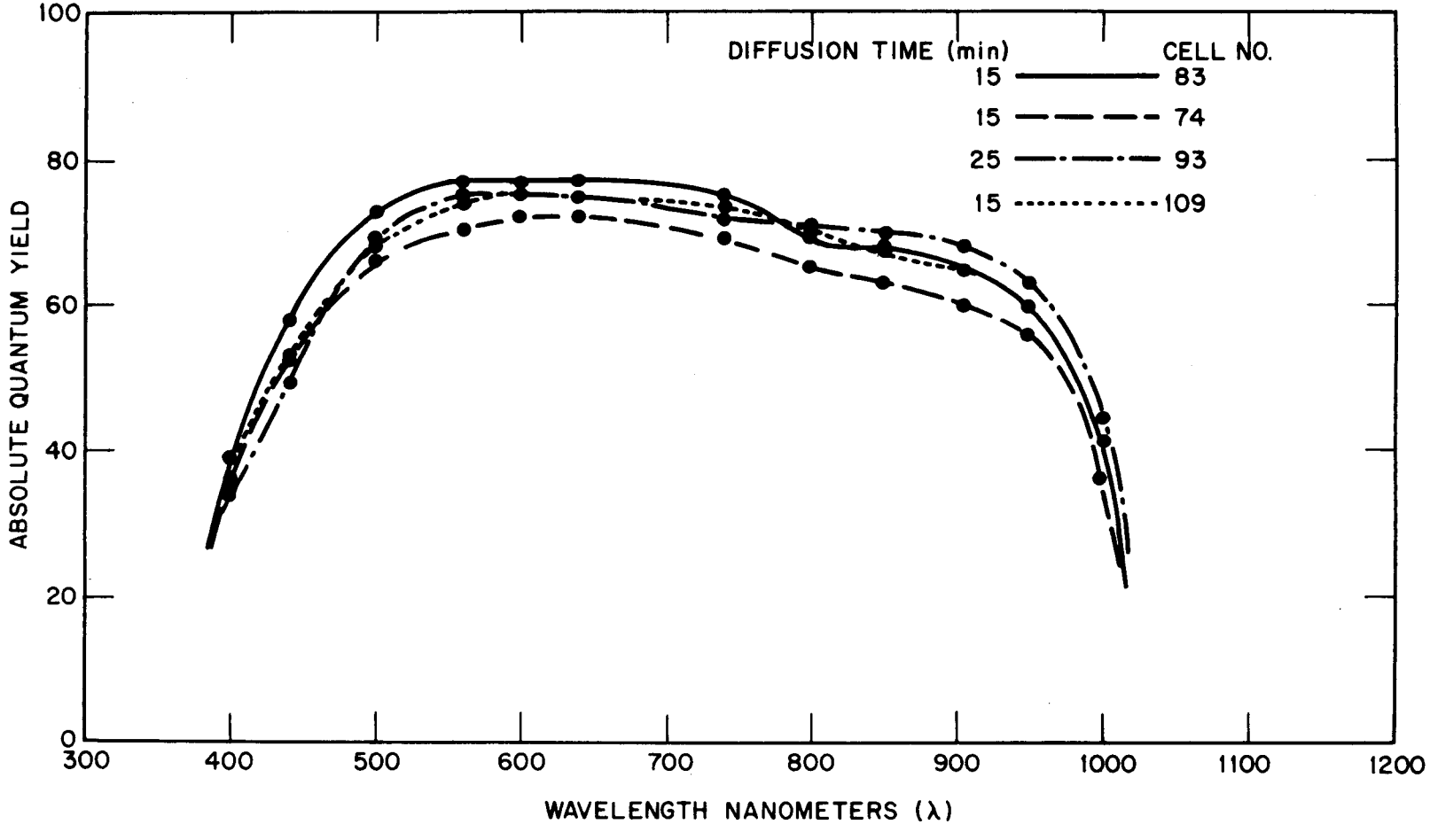


Figure 10–Quantum Yield Variations as a Function of the Diffusion Time